Nanoscale

Accepted Manuscript

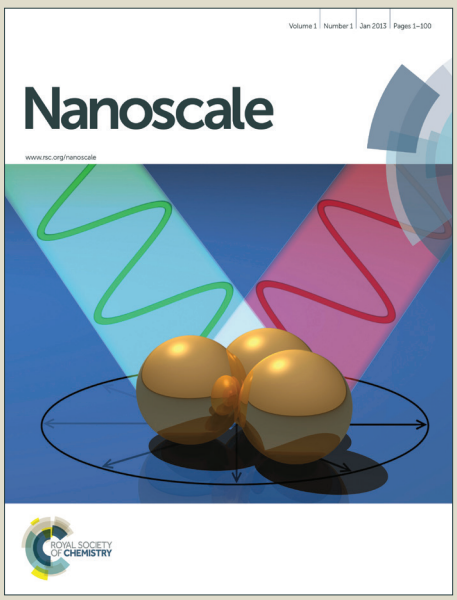

ROYAL SOCIETY OF CHEMISTRY

www.rsc.org/nanoscale

Cu-Ni Nano-Alloy: Mixed, Core-Shell or Janus Nano-Particle?

Grégory Guisbiers, Subarna Khanal, Francisco Ruiz-Zepeda, Jorge Roque de la Puente, Miguel José-Yacaman*

Department of Physics & Astronomy, University of Texas at San Antonio, One UTSA Circle, San Antonio, Texas 78249, United States of America

*E-mail: gregory.guisbiers@physics.org

ABSTRACT

Bimetallic nanoparticles like Cu-Ni are particularly attractive due to their magnetic and catalytic properties; however, their properties depend strongly on the structure of the alloy i.e. mixed, core-shell or Janus. To predict the alloy structure, this paper investigates the size and shape effects as well as the surface segregation effect on the Cu-Ni phase diagram. Phase maps have been plotted to determine the mixing/demixing behavior of this alloy according the particle shape. Cu-Ni nanoalloy can form a mixed particle or a Janus one depending on the synthesis temperature. Surface segregation is also considered and reveals a nickel surface-enrichment. Finally, this paper provides a useful roadmap for experimentalists.

TOC

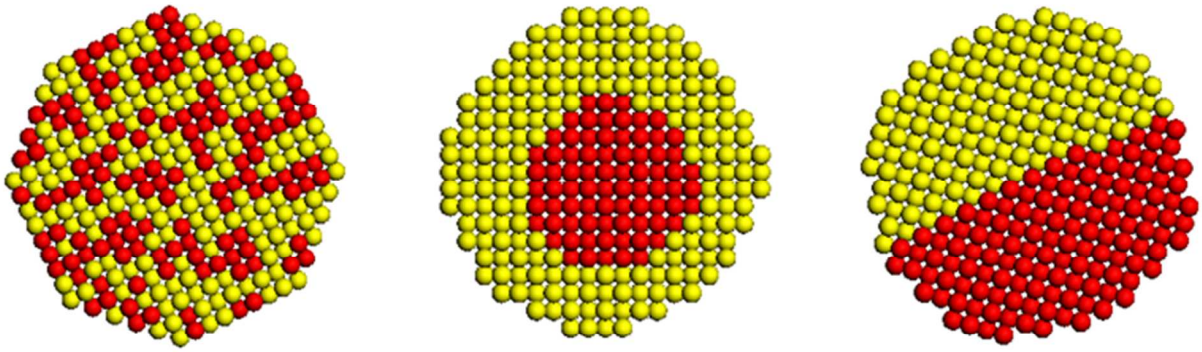

KEYWORDS : binary phase diagram, segregation, size effect, polyhedra, nano-thermodynamics, Janus nanoparticle

Cu-Ni is an important alloy in nanotechnology due to its new physical and chemical properties appearing at the nanoscale and coming from the high surface-to-volume ratio and quantum confinement[1]. Bimetallic Cu-Ni nanoparticles are used as catalysts in important chemical reactions like methane decomposition[2], ethanol steam reforming[3], oxidation of methanol[4], water-gas-shift reaction[5, 6]. Cu-Ni nanoparticles are also used in magnetic applications as the Cu-Ni core shell structure exhibits ferromagnetic properties[7].

There are only a few reports discussing the properties of Cu-Ni at the nanoscale and they all focused on the liquidus/solidus curves and considered either spherical or cubic shapes. Huang and Balbuena[8] applied molecular dynamics simulations using the Sutton-Chen many-body potential to calculate the melting behavior of cubic Cu-Ni clusters (343 atoms and 1000 atoms) at two different compositions ($Cu_{0.25}Ni_{0.75}$ and $Cu_{0.5}Ni_{0.5}$). Shirinyan *et al.*[9] used a thermodynamical approach to calculate the entire phase diagram of a spherical nanoparticle at 60 nm. Li *et al.*[10] studied, via molecular dynamics simulations using the general embedded atom method, the melting behavior of Cu-Ni clusters (2243 atoms) at three different compositions ($Cu_{0.8}Ni_{0.2}$, $Cu_{0.5}Ni_{0.5}$, $Cu_{0.2}Ni_{0.8}$). Then, the same group of authors Li *et al.*[11] studied via the same method the liquidus/solidus curves of two Cu-Ni clusters (682 and 1048 atoms). Sopousek *et al.*[12] used the CALPHAD method to calculate the liquidus/solidus curves of spherical randomly mixed nanoparticles of 10 and 20 nm in diameter. In the present paper, we predict the entire phase diagram for a variety of different polyhedra often met at the nanoscale (tetrahedron, cube, octahedron, decahedron, dodecahedron, rhombic dodecahedron, truncated octahedron, cuboctahedron, and icosahedron)[13] at sizes equal to 4 nm and 10 nm. Furthermore, we also study the surface segregation effect as function of temperature.

A standard way to predict the solid solubility of two metals is using the empirical Hume-Rothery rules[14, 15]. These rules suggest that the alloy is formed if the crystal structure, atomic radii, valence and electronegativity of the elements are similar. The Cu-Ni alloy completely fulfills all the Hume-Rothery rules and forms a substitutional solid solution. Indeed, both metals have the same crystal structure (fcc), same valence (+1), similar atomic radii (size mismatch~2%), and similar electronegativity (difference~2%). The complete miscibility and the absence of maxima/minima in the liquidus/solidus curves (Figure 1) suggest that the Cu-Ni alloy could be described as an ideal solution system. However, there exists a miscibility gap at low temperature (~630K)[1, 16] attributed to the positive values of the mixing enthalpies in the liquid and solid states[17, 18]. Therefore, to consider the chemical interactions between Cu and Ni in both the liquid and the solid phases, we use the regular solution model (i.e. a quasi-chemical model), where the solidus-liquidus curves are given by[19]:

$$\begin{cases} kT\ln\left(\dfrac{x_{solidus}}{x_{liquidus}}\right)=\Delta H_m^A\left(1-\dfrac{T}{T_m^A}\right)+\Omega_l\left(1-x_{liquidus}\right)^2-\Omega_s\left(1-x_{solidus}\right)^2 \\ kT\ln\left(\dfrac{1-x_{solidus}}{1-x_{liquidus}}\right)=\Delta H_m^B\left(1-\dfrac{T}{T_m^B}\right)+\Omega_l x_{liquidus}^2-\Omega_s x_{solidus}^2 \end{cases} \quad (1)$$

Where kT has its usual meaning. $x_{solidus}$ ($x_{liquidus}$) is the composition of the solid (liquid) phase at given temperature T. T_m^A and T_m^B are the size-dependent melting temperature of nickel and copper respectively. ΔH_m^A and ΔH_m^B are the size-dependent melting enthalpy of nickel and copper respectively. Ω_l and Ω_s are the size-dependent interactions parameters in the liquid and

solid phases respectively. The interaction parameters are related to the mixing enthalpies by the following relationship, $\Delta H_{mix,s(l)} = x_{Cu} x_{Ni} \Omega_{s(l)}$. If the interactions parameters, Ω_l and Ω_s are set to zero, we retrieve the equations describing the liquidus/solidus curves of an ideal solution. From Figure 1, it is clear that the experimental data points[20] of Cu-Ni alloy are well described by the regular solution model. Furthermore, the deviations from the ideality in the two phases are relatively small and of comparable magnitude.

To calculate the nano-phase diagram, the size-dependent properties and parameters have to be first evaluated. The size-dependent melting temperature, melting enthalpy and interactions parameters are calculated by using the same relationship (equation 2)[21], this is justified by quantum physics considerations[19, 21-23] where all thermodynamic quantities are approximately a linear function of $1/D$ (D denotes the length edge of the polyhedron) that corresponds to the surface-to-volume ratio of the nanoparticle.

$$\frac{\Phi}{\Phi_\infty} = 1 - \frac{\alpha}{D} \qquad (2)$$

Let us note the nano-scaled property/parameter as Φ and the corresponding bulk property/parameter as Φ_∞. The shape-dependent parameter, α, is defined as $\alpha = \left[N_{surf} \Big/ \left(N_{tot} X_{(hkl)} a \right) \right] \left(\gamma_s - \gamma_l \right) \Big/ \Delta H_{m,\infty}$ where $X_{(hkl)}$ is a numerical constant equal to ½, $\sqrt{2}/4$, $\sqrt{3}/3$ for a 100, 110 and 111 face; N_{surf}/N_{tot} is the ratio between the surface atoms number to the total atoms number; γ_l and γ_s are the surface energies in the liquid and solid state respectively;

a is the bulk lattice parameter. In a first approximation, the surface energies and the lattice parameter are considered size-independent. This is justified by the fact that we restrict our discussion to size above 4 nm where these corrections are negligible. Explicitly, the lattice parameter is reduced by ~1% for size around 4 nm[22] and surface energy is reduced by ~10% for size around 4 nm[23]. Generally, the solid surface energy is not well determined in contrast to the liquid surface energy which is quite accurately accessible experimentally[24]. Moreover, this is the difference between surface energies which is involved in the definition of α, meaning that in the case of nickel (copper) if we consider a 10% size effect on the surface energies, the difference, $\gamma_{s,(111)} - \gamma_l$, decreases by about ~3% (~6%) compared to the bulk case, and can therefore be considered as a second order correction.

Introducing the size-dependent properties, T_m^A, T_m^B, ΔH_m^A, ΔH_m^B, and parameters, Ω_l, Ω_s, calculated at a given size (4 nm and 10 nm) by equation 2, into the set of equations (1), we can predict the phase diagram of Cu-Ni at the nanoscale (Figure 2). All the phase diagrams at 4 nm and 10 nm show that the liquid region is enlarged and the solid solution area is narrowed. Above the liquidus curve, this is a one-phase field where the solution is purely liquid. In the lens-shape region, this is a two-phase field where the liquid is at equilibrium with the solid phase. Below the solidus curve, this is a one-phase field where the solution is purely solid. Within the solid solution, the miscibility gap is also reduced when size is decreased due to a lower value for the size-dependent interactions parameters. This is an illustration of the degradation of the regular solution into an ideal solution when size decreases. This phenomenon has already been noticed by Jiang *et al.*[19].

From the miscibility gap, we define the miscibility temperature as the critical temperature below which both constituents are no more miscible. As can be seen from figure 2, the miscibility temperature is size and shape dependent. Plotting the miscibility temperature for each polyhedron as a function of the number of faces gives access to a phase map indicating the mixing-demixing behavior of the Cu-Ni (Figure 3). Above the miscibility temperature, the alloy is formed while below this temperature the Janus particle is formed. These phase maps, plotted at sizes equal to 4 nm and 10 nm, are very informative for experimentalists who can adjust their synthesis temperature or adjust the heating treatment after the synthesis, according the type of nanoparticle they want to produce. Cu-Ni nanoalloy is very difficult to synthesize at room temperature and generally requires a heat treatment[7, 25-28]. For the tetrahedron having a side edge length ~ 4 nm (figure 2), the miscibility gap disappears completely meaning that there is no phase separation in the solid solution. In the case of a bimetallic alloy, it is interesting to consider the surface segregation. Indeed, due to a higher surface-to-volume ratio[29], diffusion is enhanced in nano-alloys compared to bulk alloys leading to a possible core-shell formation. Diffusion of atoms from the bulk to the surface is attributable to the gradient of the chemical potential between the bulk and the surface[30]. The solidus and liquidus compositions of the alloy can then be determined at the surface by using the William-Nason's model[31]:

$$x_{solidus}^{surface} = \frac{\frac{x_{solidus}^{core}}{1-x_{solidus}^{core}} e^{-\frac{\Delta H_{sub} z_{1v}}{z_1 kT}}}{1+\frac{x_{solidus}^{core}}{1-x_{solidus}^{core}} e^{-\frac{\Delta H_{sub} z_{1v}}{z_1 kT}}} \quad (3)$$

$$x_{liquidus}^{surface} = \frac{\frac{x_{liquidus}^{core}}{1-x_{liquidus}^{core}} e^{-\frac{\Delta H_{vap} z_{1v}}{z_1 kT}}}{1+\frac{x_{liquidus}^{core}}{1-x_{liquidus}^{core}} e^{-\frac{\Delta H_{vap} z_{1v}}{z_1 kT}}} \quad (4)$$

Where $x_{solidus}^{core}$ and $x_{liquidus}^{core}$ are the bulk solidus and liquidus composition given by the set of equations (1) i.e. when segregation is not considered. $\Delta H_{vap} = \left|\Delta H_{v,A} - \Delta H_{v,B}\right|$ is the absolute difference in the enthalpy of vaporization of the two pure elements. $\Delta H_{sub} = \left|\Delta H_{s,A} - \Delta H_{s,B}\right|$ is the absolute difference in the enthalpy of sublimation of the two pure elements. z_{1v}/z_v is the fraction of nearest neighbor atoms missing for atoms in the first layer (for atoms belonging to a 111 face in a fcc structure, $z_{1v}/z_v = 0.25$). Considering surface segregation on the solidus/liquidus curves, it is clear from figure 4 that nickel is preferentially found at the surface of the nanoalloy.

Experimentally, we have synthesized Cu-Ni nanoparticles using wet chemistry methods at 250°C (see supplementary information for details) and characterized by transmission electron microscopy (TEM) in STEM mode. This has been carried out on a JEOL ARM200F probe aberration corrected electron microscope operating at 200 kV. The samples for TEM observations were prepared by dropping the colloidal solution onto gold TEM grids and drying in air. STEM images were recorded by High Angle Annular Dark Field (HAADF) (Figure 5 a-b). The Z-contrast images whose signal intensity depends on the atomic number[32], show that copper atoms appear brighter than nickel ones, evidencing an alloyed and a Janus particle structure on Figures 5a and 5b, respectively. The elemental distribution of Cu and Ni inside the alloy was analyzed by Energy Dispersive X-ray Spectroscopy (EDX) with an EDAX Apollo XLT-2

Silicon drift detector. EDX line scan taken over the Cu-Ni nanoparticles is presented in Figure 5c-d. The intensity of the copper and nickel peaks differ according the position in the particle, confirming the Janus structure of the particle. From Figure 5, it is clear that the Cu-Ni nanoparticles synthesized at 250°C adopt the structure of Janus particles confirming the theoretical predictions shown on Figure 3. Furthermore, nickel surface segregation is also observed in figure 5b confirming then the theoretical calculations.

Finally, using nano-thermodynamics theory, we confirm that mixed Cu-Ni nanoparticles are difficult to synthesize at room temperature and require a substantial heat treatment to be produced. By adjusting the value of the synthesis temperature, it is possible to control the structure of the alloy. By reducing the size of the nanoparticle, the miscibility gap narrows and the mixing/demixing behavior of the Cu-Ni nanoparticle can be predicted. It is also found that nickel preferentially segregates at the surface of the particle. To conclude, this paper contains the first phase map indicating the mixed or Janus structure of Cu-Ni nanoalloy according the shape of the particle. For sure, this will help the experimentalists by guiding them in their attempts to synthesize Cu-Ni nanoparticles with the desired structure.

Acknowledgments

This project was supported by grants from the National Center for Research Resources (G12RR013646-12) and the National Institute on Minority Health and Health Disparities (G12MD007591) from the National Institutes of Health. The authors would also like to acknowledge the NSF PREM #DMR0934218 and the Mexican Council for Science and Technology, CONACYT (Mexico) through the project 207725.

Table 1. Material Properties used to Calculate the Phase Diagrams at the Nanoscale.

Material properties	Ni	Cu
Crystal structure[33]	fcc	fcc
$T_{m,\infty}$ (K)[33]	1728	1357
$\Delta H_{m,\infty}$ (J/mol)[33]	17480	13263
γ_l (J/m²)[33]	1.725	1.300
$\gamma_{s,111}$ (J/m²)[34]	2.011	1.952
$\gamma_{s,100}$ (J/m²)[34]	2.426	2.166
$\gamma_{s,101}$ (J/m²)[34]	2.368	2.237
Ω_l (J) [35]	12219	
Ω_s (J) [35]	11376	
Atomic radii (pm)[33]	115	117
Electronic affinity (eV)[33]	1.16	1.24
1st ionization energy (eV)[33]	7.64	7.73
χ, Mulliken electronegativity	4.40	4.49

(eV)*		
$\Delta H_{v,\infty}$, Molar heat of vaporization (J/mol)[33]	369240	300700

*The Mulliken electronegativity is defined as the mean value between the electronic affinity and the first ionization energy.

FIGURES CAPTIONS

Figure 1. Binary phase diagram (temperature versus composition) of bulk Cu-Ni alloy. The diagram consists of two single-phase fields separated by a two-phase field with a miscibility gap at low temperatures. The experimental points come from Ref.[20].

Figure 2. Binary phase diagrams of Cu-Ni alloys for different shapes: a) tetrahedron, b) cube, c) octahedron, d) decahedron, e) dodecahedron, f) truncated octahedron, g) cuboctahedron, h) icosahedron, i) rhombic dodecahedron.

Figure 3. Mixing-demixing phase map for nanoparticle having a side edge length equal to a) 4 nm and b) 10 nm. These phase maps represent the miscibility temperature versus the number of facets of each polyhedron considered in this study. The squares represent the experimental data i.e. the synthesized nanoparticles shown on Figure 5. The temperature used to synthesize these Cu-Ni nanoparticles was 250 K as indicated by the red arrow.

Figure 4. a) Binary phase diagram of a spherical Cu-Ni nanoparticle (diameter = 15 nm) without and with surface segregation. The solidus-liquidus curves describing the segregated nanoparticle reveals the nickel surface enrichment. b) STEM image of a "nearly" spherical Cu-Ni nanoparticle having a diameter around ~15nm. The red arrow indicates the scan direction. c) EDX line scan across this particle revealing the nickel surface enrichment.

Figure 5. STEM images of Cu-Ni nanoparticles : a) HAADF image of three cubic nanoparticles, b) HAADF image of a "nearly" decahedral nanoparticle. c) EDX line scan on one of the cubic nanoparticles shown in a), illustrating the alloy behavior of the nanoparticle. d) EDX line scan on the "nearly" decahedral nanoparticle shown in b), illustrating the Janus behavior of the nanoparticle. The red arrows in a) and b) indicate the scan direction.

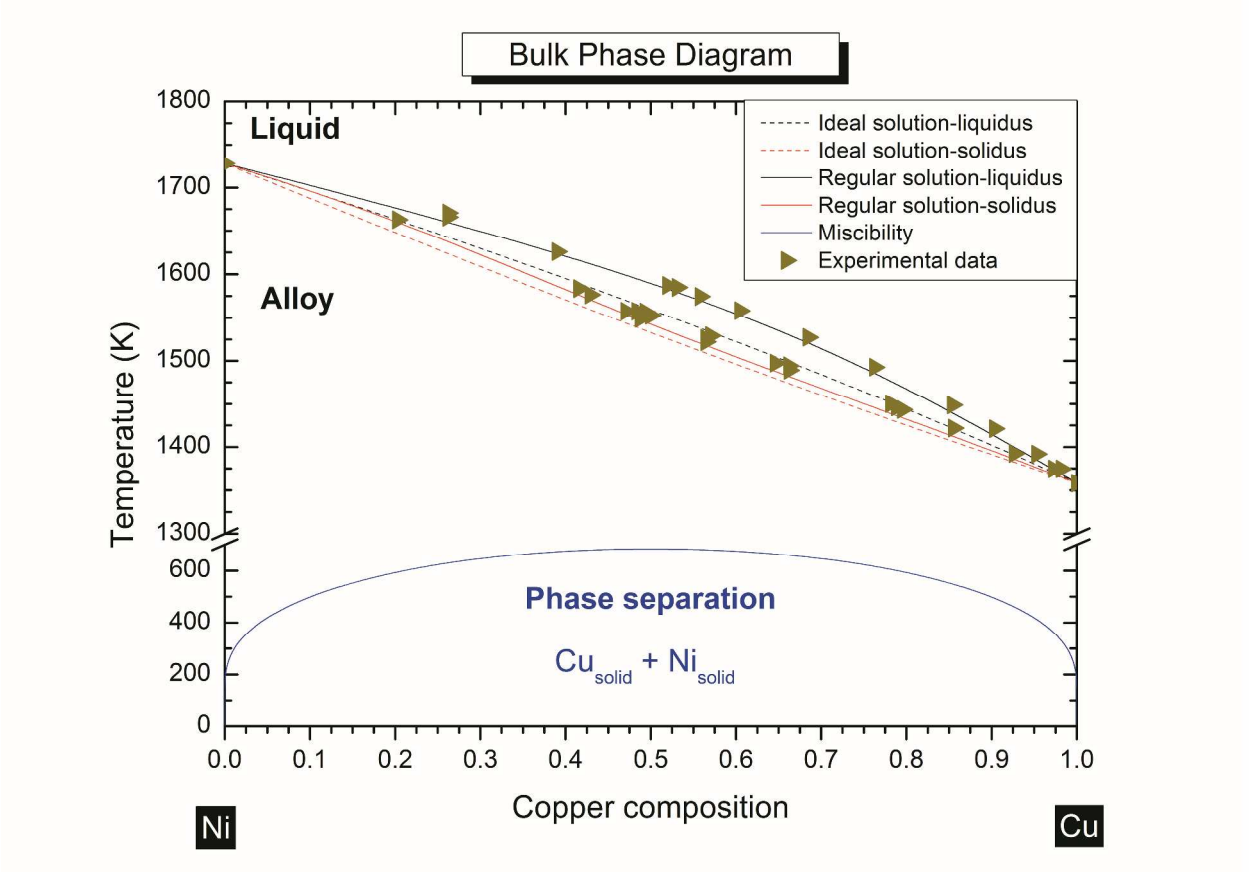

Figure 1

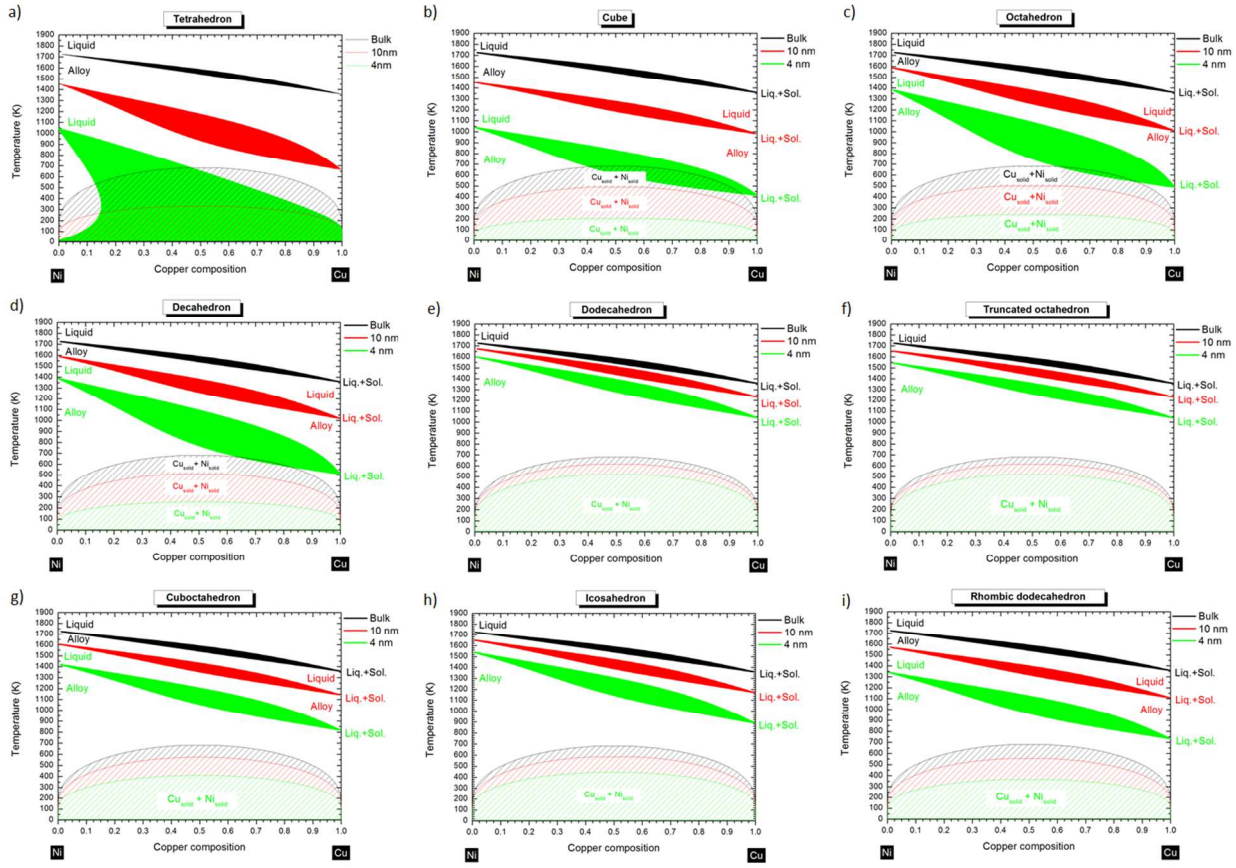

Figure 2

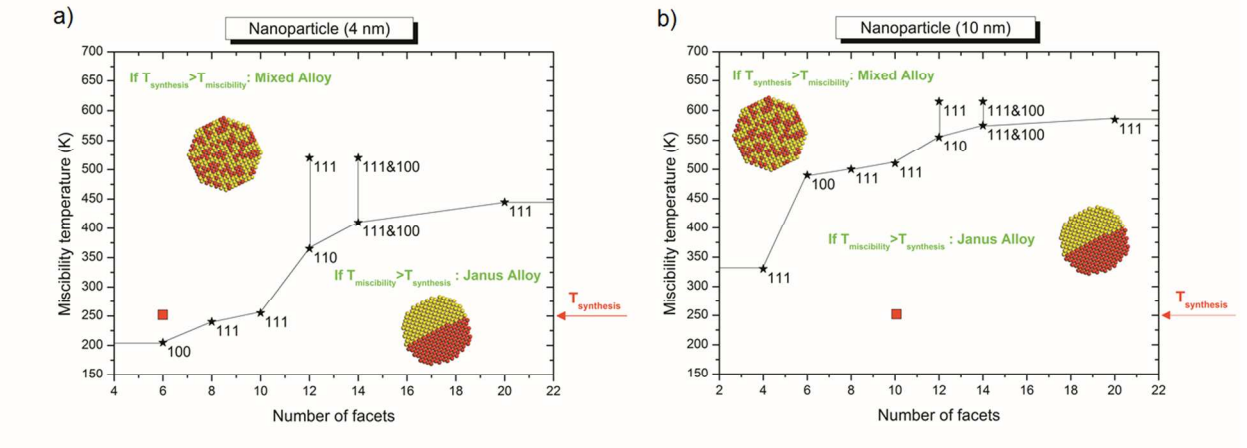

Figure 3

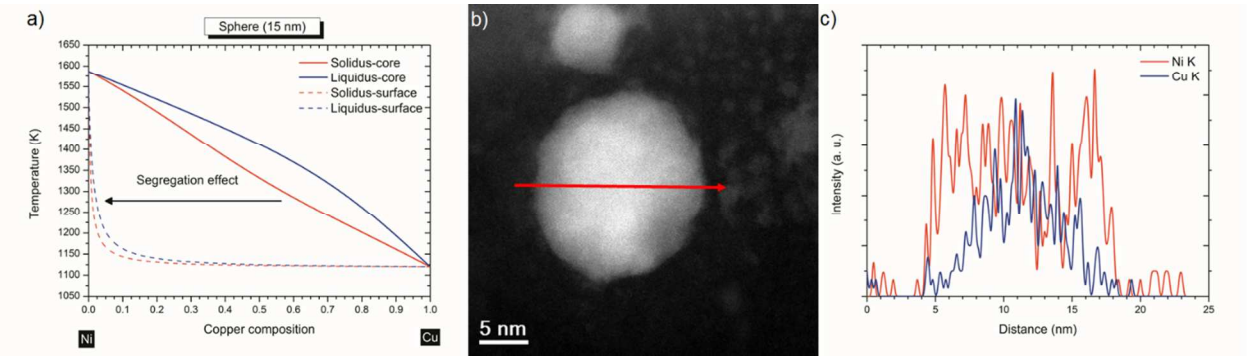

Figure 4

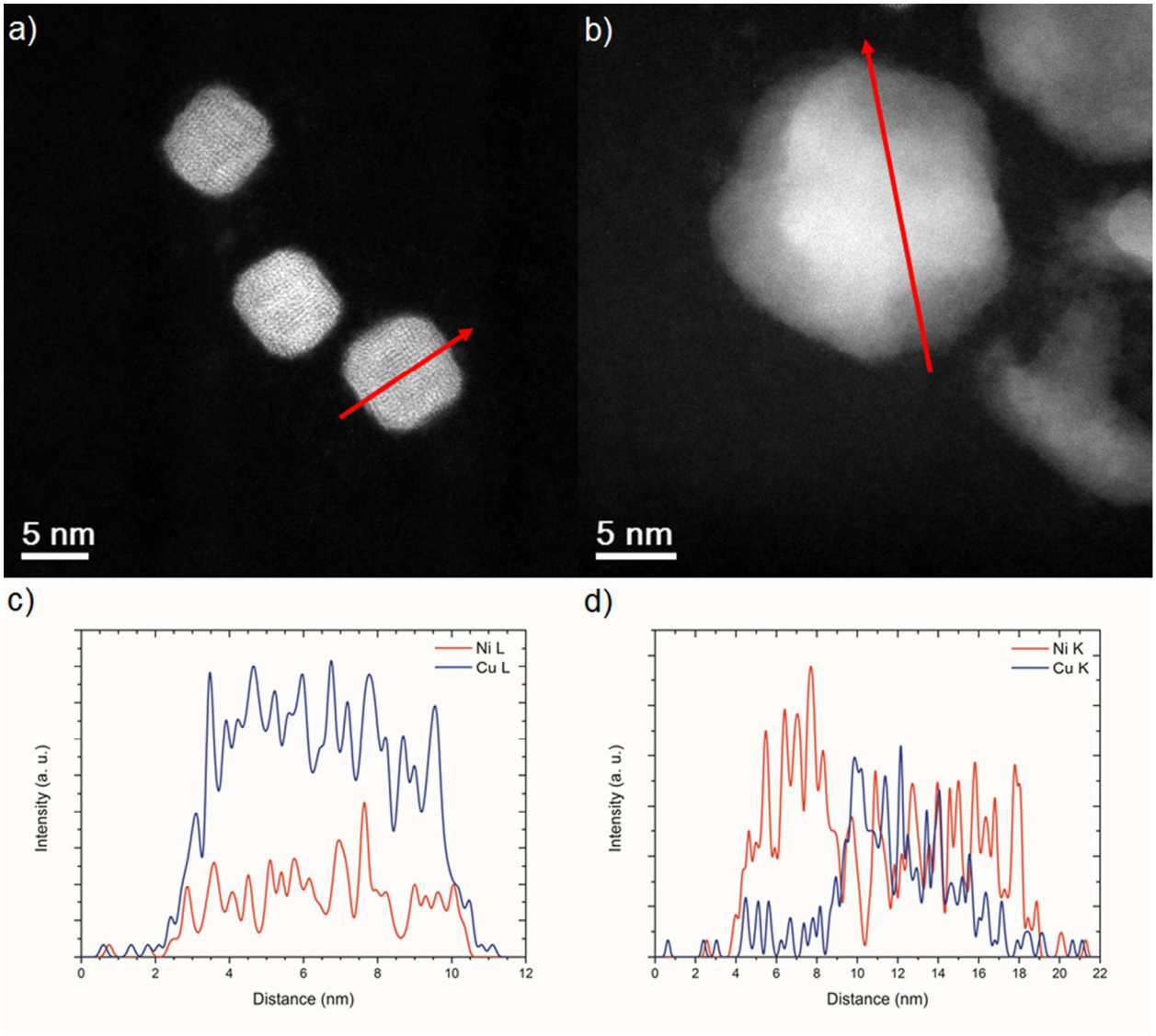

Figure 5

REFERENCES

1. R. Ferrando, J. Jellinek and R. L. Johnston, *Chemical Reviews*, 2008, 108, 845-910.
2. T. V. Reshetenko, L. B. Avdeeva, Z. R. Ismagilov, A. L. Chuvilin and V. A. Ushakov, *Applied Catalysis A: General*, 2003, 247, 51-63.
3. A. J. Vizcaíno, A. Carrero and J. A. Calles, *International Journal of Hydrogen Energy*, 2007, 32, 1450-1461.
4. M. Jafarian, R. B. Moghaddam, M. G. Mahjani and F. Gobal, *Journal of Applied Electrochemistry*, 2006, 36, 913-918.
5. J.-H. Lin and V. V. Guliants, *Applied Catalysis A: General*, 2012, 445-446, 187-194.
6. J.-H. Lin, P. Biswas, V. V. Guliants and S. Misture, *Applied Catalysis A: General*, 2010, 387, 87-94.
7. T. Yamauchi, Y. Tsukahara, T. Sakata, H. Mori, T. Yanagida, T. Kawai and Y. Wada, *Nanoscale*, 2010, 2, 515-523.
8. S.-P. Huang and P. B. Balbuena, *Journal of Physical Chemistry B*, 2002, 106, 7225-7236.
9. A. Shirinyan, M. Wautelet and Y. Belogorodsky, *Journal of Physics: Condensed Matter*, 2006, 18, 2537-2551.
10. G. Li, Q. Wang, D. Li, X. Lü and J. He, *Materials Chemistry and Physics*, 2009, 114, 746-750.
11. G. Li, Q. Wang, T. Liu, K. Wang and J. He, *Journal of Cluster Science*, 2010, 21, 45-55.
12. J. Sopousek, J. Vrestal, J. Pinkas, P. Broz, J. Bursik, A. Styskalik, D. Skoda, O. Zobac and J. Lee, *CALPHAD: Computer Coupling of Phase Diagrams and Thermochemistry*, 2014, 45, 33-39.
13. M. J. Yacaman, J. A. Ascencio, H. B. Liu and J. Gardea-Torresdey, *Journal of Vacuum Science & Technology B*, 2001, 19, 1091-1103.
14. W. Hume-Rothery, G. W. Mabbott and K. M. Channel Evans, *Philosophical Transactions of the Royal Society London Series A*, 1934, 233, 1-97.
15. U. Mizutani, *Hume-Rothery Rules for Structurally Complex Alloy Phases*, CRC Press, 2011.
16. K. P. Gupta, *Journal of Phase Equilibria and Diffusion*, 2009, 30, 651-656.
17. J. Lee, J. Park and T. Tanaka, *CALPHAD: Computer Coupling of Phase Diagrams and Thermochemistry*, 2009, 33, 377-381.
18. T. Tanaka and S. Hara, *Zeitschrift Fur Metallkunde*, 2001, 92, 1236-1241.
19. Q. Jiang and Z. Weng, *Thermodynamics of Materials*, Springer, 2011.
20. E. A. Feest and R. D. Doherty, *Journal of the Institute of Metals*, 1971, 99, 102-103.
21. G. Guisbiers and G. Abudukelimu, *Journal of Nanoparticle Research*, 2013, 15, 1431.
22. W. H. Qi and M. P. Wang, *Journal of Nanoparticle Research*, 2005, 7, 51-57.
23. S. Y. Xiong, W. H. Qi, Y. J. Cheng, B. Y. Huang, M. P. Wang and Y. J. Li, *Physical Chemistry Chemical Physics*, 2011, 13, 10648-10651.
24. G. Guisbiers, S. Arscott and R. Snyders, *Applied Physics Letters*, 2012, 101.
25. M. D. Cangiano, A. C. Carreras, M. W. Ojeda and M. D. Ruiz, *Journal of Alloys and Compounds*, 2008, 458, 405-409.

26. E. L. de Leon Quiroz, D. Vasquez Obregon, A. Ponce Pedraza, M. J. Yacaman and L. A. Garcia-Cerda, *IEEE Transactions on Magnetics*, 2013, 49, 4522-4524.
27. M. D. Cangiano, M. W. Ojeda, A. C. Carreras, J. A. Gonzalez and M. D. Ruiz, *Materials Characterization*, 2010, 61, 1135-1146.
28. C. Damle and M. Sastry, *Journal of Materials Chemistry*, 2002, 12, 1860-1864.
29. G. Guisbiers and L. Buchaillot, *Nanotechnology*, 2008, 19, 435701.
30. H. Mehrer, *Diffusion in Solids*, Springer, 2007.
31. F. L. Williams and D. Nason, *Surface Science*, 1974, 45, 377-408.
32. S. J. Pennycook, *Ultramicroscopy*, 1989, 30, 58-69.
33. W. Martienssen and H. Warlimont, *Springer handbook of condensed matter and materials data*, Springer, 2005.
34. L. Vitos, A. V. Ruban, H. L. Skriver and J. Kollar, *Surface Science*, 1998, 411, 186-202.
35. L. H. Liang, D. Liu and Q. Jiang, *Nanotechnology*, 2003, 14, 438-442.